Deposition of phosphate coatings on titanium within scaffold structure

BARTŁOMIEJ TRYBUŚ[1], ANDRZEJ ZIELIŃSKI[1]*, RENE BEUTNER[2],
TOMASZ SERAMAK[1], DIETER SCHARNWEBER[2]

[1] Gdańsk University of Technology, Gdańsk, Poland.
[2] Technische Universität Dresden, Dresden, Deutschland.

Purpose: Existing knowledge about the appearance, thickness, and chemical composition of phosphate coatings on titanium inside porous structures is insufficient. Such knowledge is important for the design and fabrication of porous implants.

Methods: Metallic scaffolds were fabricated by selective laser melting of 316L stainless steel powder. Phosphate coatings were deposited on Ti sensors placed either outside the scaffolds or in the holes in the scaffolds. The electrochemically-assisted cathodic deposition of phosphate coatings was performed under galvanostatic conditions in an electrolyte containing the calcium and phosphate ions. The phosphate deposits were microscopically investigated; this included the performance of mass weight measurements and chemical analyses of the content of Ca^{2+} and PO_4^{2-} ions after the dissolution of deposits.

Results: The thicknesses of the calcium phosphate coatings were about 140 and 200 nm for isolated titanium sensors and 170 and 300 nm for titanium sensors placed inside pores. Deposition of calcium phosphate occurred inside the pores up to 150 mm below the scaffold surface. The deposits were rich in Ca, with a Ca/P ratio ranging from 2 to 2.5.

Conclusions: Calcium phosphate coatings can be successfully deposited on a Ti surface inside a model scaffold. An increase in cathodic current results in an increase in coating thickness. Any decrease in the cathodic current inside the porous structure is slight. The calcium phosphate inside the pores has a much higher Ca/P ratio than that of stoichiometric HAp, likely due to a gradual increase in Ca fraction with distance from the surface.

Key words: phosphate coatings, electrochemical deposition, stainless steel, selective laser melting, titanium

1. Introduction

Load-bearing implants of different kinds are made of metallic alloys such as stainless steel, titanium, cobalt, and Ni-Ti alloys. Porous metallic implants and biodegradable metals have often been considered and investigated for two reasons: (i) they permit bone tissue to grow into the implant, enhancing its stabilisation, and (ii) they possess a lower Young's modulus, closer to that of bone, thus reducing the 'screening effect'. Porous implants have been developed especially for titanium and its alloys based on several techniques [23] and, recently, often with a 3D printing [2], [12], [13], [18]. The titanium dioxide scaffolds have also been produced [21].

The porous stainless steel 316L, used in this research for a model scaffold, has also been produced in different ways for medical purposes. Conventional sintering was used [7] to produce the steel with porosity ranging from 21% to 55%, while laser sintering became useful to made the steel of similar, 40–50% porosity [5]. Selective laser sintering in a hydrogen atmosphere was used [25] to produce 316L steel from powder coated with an ethylene-vinyl acetate copolymer. After sintering at 1100–1300 °C,

the average pore size 160–35 μm, porosity 58–28%, elastic modulus 1.58–6.64 GPa and compressive yield strength 15.5–52.8 MPa were found. The europium doped TiO_2 sol was deposited on 316L steel plates by either dip-coating or spin-coating method to protect the steel from an aggressive environment [6].

A variety of techniques are used to deposit phosphate coatings. For titanium and its alloys, these include electrochemically assisted deposition (ECAD) [22], [27], electrophoretic deposition [1], [16], biomimetic methods [3], [18], [20], magnetron sputtering [8], [17], ion-beam physical vapour deposition [9], the alternate immersion method [11], [24], and pulsed laser deposition [20], [23].

Deposition of phosphate coatings inside metallic scaffolds has seldom been investigated. In [10], calcium phosphate coatings inside a porous titanium alloy were produced using both biomimetic deposition (BD) and ECAD methods in aqueous solutions. The BD coatings were thicker and more uniform than the ED coatings, but the ED method was less sensitive to the condition of the titanium surface and much faster in terms of the deposition of the coating. The same technique was used to prepare BD hydroxyapatite coatings in porous CoCr substrates manufactured by electron beam melting [15]. In [26], microporous and macroporous titanium samples produced by powder metallurgy were immersed in a solution containing calcium and phosphorus ions, resulting in the appearance of globular or plate-like coatings typical of hydroxyapatite and octacalcium phosphate. The positive influence of calcium ion deposition on the apatite-inducing ability of porous titanium was demonstrated in [4]; a thin layer of calcium titanate/calcium oxide mixture with a nanostructured porous network was produced after hydrothermal treatment.

The present research was aimed at establishing the appearance of phosphate coatings on titanium surfaces deep inside a porous metallic structure, along with determining the thickness and chemical composition of coatings related to certain process parameters. As such measurements are difficult to carry out on a titanium scaffold, titanium sensors placed inside porous structures made of 316L stainless steel were used. This was a reasonable choice, as the deposition of phosphate is more difficult on stainless steel than on titanium. The study was expected to answer the question whether the bioactive hydroxyapatite coatings may be effectively deposited within the titanium scaffolds.

2. Materials and methods

2.1. Preparation of sensors

The sensors were wires 0.98 mm in diameter, made of Ti Grade 4. The wires were covered with isolating paint that protected the upper part from current flow and calcium phosphate deposition. The end parts of the wires were left unpainted. The sensors used different in the length the unpainted part and the lower part exposed to the solution: 5, 10, and 14 mm. The unpainted areas of the sensors were 16.1, 31.5 and 43.8 mm^2.

2.2. Preparation of scaffolds

The porous structures were made of 316L stainless steel powder. The chemical composition of the stainless steel, according to the manufacturer's attestation, is shown in Table 1. The size of each powder particle was around 25 μm. The porous structures were designed using Autodesk Inventor software; scaffolds were produced using an additive technique, through selective laser melting of metallic powder with Realizer II equipment. The porous structures are shown in Fig. 1, both as CAD designs and as laser-melted samples. The dimensions of the structures were $10 \times 10 \times 15$ mm; the dimension of a single hole was 0.6×0.6 mm; the number of holes in the top section was 11×11, in the side section 11×16. The same configuration was designed for every layer, from bottom to top. The actual surface area was calculated for each scaffold structure (for a perfect scaffold without a hole for a sensor) as 4727 mm^2.
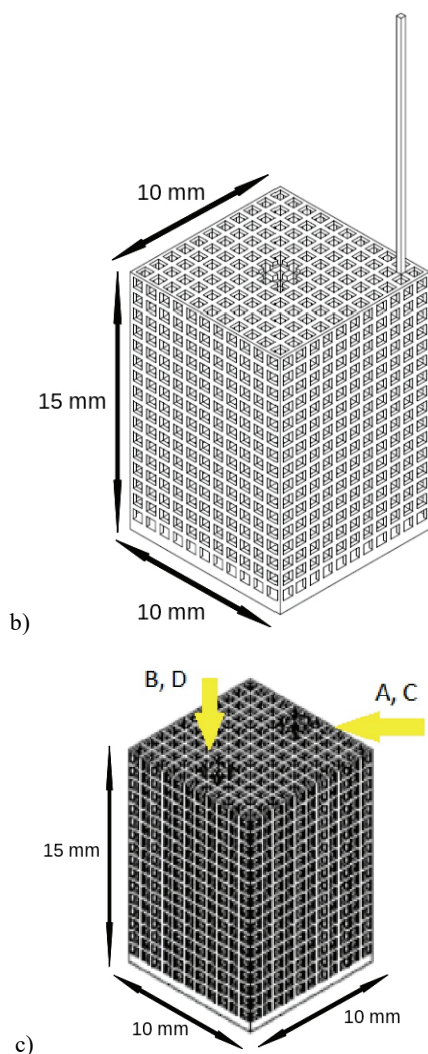
The views of different scaffolds and positions of sensors are shown in Fig. 1a–c. The sensor placement was as follows: specimen A – hole closer to the middle of sample, B – hole closer to the edge, C – hole closer to the middle, D – hole closer to the edge.

Table 1. Chemical composition of 316L steel

Element	C	Si	Mn	P	S	N	Cr	Mo	Ni
Mass %	<0.03	<1.0	<2.0	<0.045	<0.015	<0.011	16.6–18.5	2.0–2.5	10.0–13.0

ambient temperatures. The specimens were then dried in cold air.

2.3. Deposition of phosphate coatings on isolated sensors

Deposition of calcium phosphate coatings was done by means of electrochemically assisted deposition (ECAD). The solution contained 1.67 mN of calcium and 1.0 mN of phosphate ions and a 1% NH. The solution was used to set the pH at 6.4.

The scheme of change in current is shown for one selected value, 5 mA/cm^2, in Fig. 2. Three different upper cathodic current density values were used: 5, 6 and 7 mA/cm^2. The sequence of current change was as follows: initially, 10 s at open circuit potential (OCP); deposition for 60 s at 5, 6 or −7 mA/cm^2; and, finally, 60 s at OCP. This cycle was repeated ten times followed by final deposition at −8 mA/cm^2 for 5 min. The deposition temperature was 36 °C. The sample was rotated at 30 rpm for 25 min, starting after the first cycle (130 s).
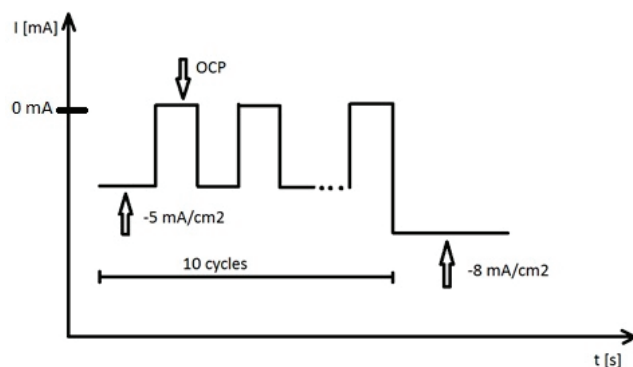

Fig. 2. Diagram presenting deposition current as a function of time. OCP – Open Circuit Potential

2.4. Deposition of phosphate coatings on sensors placed in porous specimens

Before the tests, the bottom surface of each scaffold was covered with "Deguform" silicone paint. The sensors were then placed inside the holes, their unpainted parts close to the bottom of the specimen. The same solution and deposition parameters were used for both isolated sensors and scaffolds with sensors inside.

The specimens were not fully immersed, so as to enable transport processes in the porous structure in the *x* and *y* directions (lateral) only. Under these experimental conditions, the deposition of calcium phos-

Fig. 1. View of different scaffolds (a), image of the scaffold with an SS wire designed to connect sample with a potentiostat (b), position of sensors inside the samples shown in Figs. 7–10 (c)

After completing the fabrication process and cutting the supports of the bottom part, the porous specimens were cleaned to remove loose powder particles. The process was carried out in an ultrasonic washer for 15 minutes in acetone and 45 minutes in ethanol at

phate was not expected to depend on the z position (vertical), on either the porous scaffold or the sensor electrode. Thus, a quantitative analysis of the coating deposited on the sensor electrode would enable the characterization of the transport processes driving deposition at a given position of the sensor as described by the x and y position in the porous scaffold. The holes for sensors were left above electrolyte level so that 75% of the volume of each sample was immersed. The unpainted part of the sensor was fully immersed.

The results obtained on isolated sensors of different length of the unpainted part and different current density were not very different from each other. Therefore, the tests on scaffolds were made only for selected values of those two parameters: 10-mm length of the sensor's unpainted part and –5 mA/cm^2 of the value upper current density.

2.5. Chemical analysis of coatings

After deposition, the protective paint was removed from the surface of the sensors with acetone. The sensors were then cleaned and dried in cold air. The phosphate coating was then dissolved in 400 µl of l% HNO$_3$ solution for 20 minutes. Chemical analysis of the calcium phosphate coatings was performed following their dissolution in 0.1 N nitric acid using a Calcium CPC kit (Analyticon Biotechnologies AG, Germany) and a Phosphate FS kit (DiaSys Greiner GmbH, Germany), according to the manufacturer's instructions.

2.6. Microscopic examinations

Microscopic examinations were made with a Philips XL-30 environmental scanning electron microscope (ESEM). The observations were made on isolated sensors removed from the scaffold and drained in laboratory air.

3. Results

3.1. Deposition of calcium phosphate coatings on isolated sensors

Figure 3 shows a summary of mean values of the Ca^{+2} ion mass/surface ratio; Fig. 4, of the PO$_4^{-3}$ ion mass/surface ratio; Fig. 5, the HAp mass/surface ratio, based on the Ca amount and assuming the stoichiometry

of hydroxyapatite; and Fig. 6, the Ca^{+2}/PO$_4^{-3}$ (also designated as Ca/PO$_4$) mass/surface ratio. The error was calculated based on measurements for three sensors of the same working gauge and four repetitions of chemical analysis. The calcium phosphate coating thicknesses were 156, 201, and 137 nm for unpainted parts of sensor with lengths of 5, 10, and 14 mm at –5 mA/cm^2, respectively; 178, 159, and 109 nm at –6 mA/cm^2, respectively; and 191, 181, and 156 nm at –7 mA/cm^2, respectively. These calculations were based on two assumptions: (i) the coatings were homogenous and non-porous, and (ii) calcium phosphate is a stoichiometric hydroxyapatite.
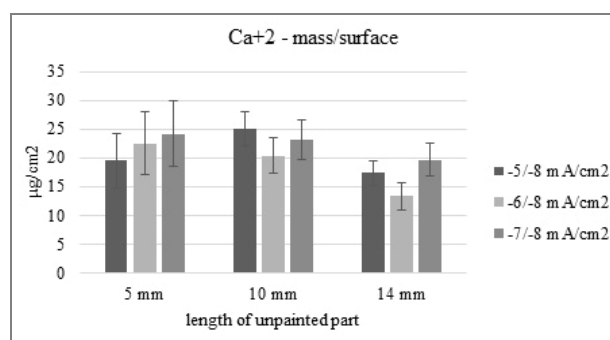

Fig. 3. Calcium ions mass/surface ratio for deposition on isolated sensors
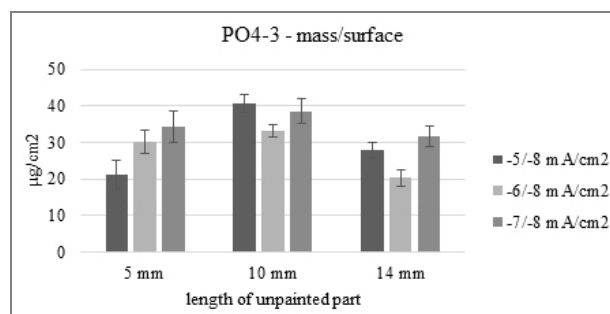

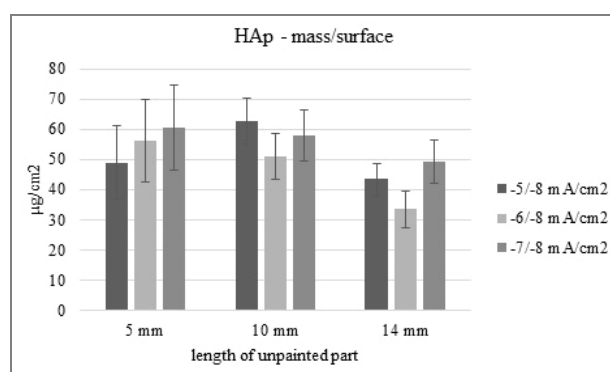Fig. 4. Phosphate ions mass/surface ratio for deposition on isolated sensors

Fig. 5. Hydroxyapatite mass/surface ratio for deposition on isolated sensors (calculated based on Ca values)
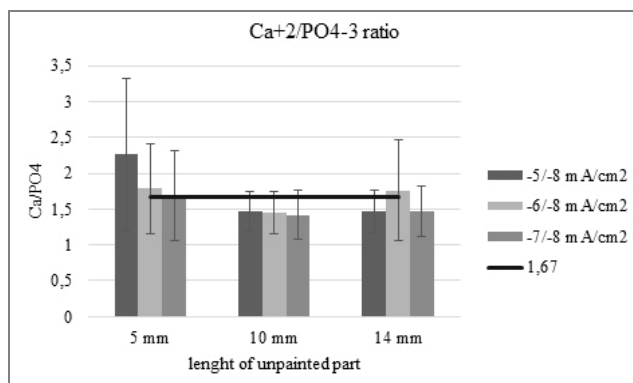
Fig. 6. Ca^{2+}/PO_4^{-3} ion ratio
for deposition on isolated sensors

Fig. 7. Calcium mass/surface ratio
on sensors inside porous structure

The intrinsic structure of electrochemically deposited HAp coatings was shown to be homogenous and demonstrated only surface roughness on flat specimens. The results illustrate the deposit mass as a function of both current density and length of the sensor. The composition of the coatings was close to that of hydroxyapatite. Therefore, the errors resulting from the above assumptions are low and the deviations of obtained thickness values from the calculated values may be estimated at 3–5%. Within the limits of those experimental errors, it may then be concluded that the current regime and length of the unpainted part have moderate effects on deposit masses.

3.2. Deposition on sensors inside scaffold specimens

The sensor position inside the scaffold is shown in Fig. 1. The obtained results, presented in Figs. 7–10, are close to those obtained for isolated sensors in terms of the mass content of calcium and phosphate ions. The thicknesses of coatings, calculated from the Ca mass measurements, were in the range from 170 to 300 nm, on the assumptions given in Section 3.1. However, the Ca/P ratios were well above stoichiometric value and for that reason, the true thickness of the phosphate coatings should likely be 140–240 nm. Moreover, as illustrated by the surfaces covered with calcium phosphate coatings (Fig. 11), the porous coatings always appeared, presumably as the effect of hydrogen evolution. Assuming the porosity as approaching even 10%, the real thickness could be finally between some 154 and 264 nm. No significant effect of sensor position on the obtained results was observed.
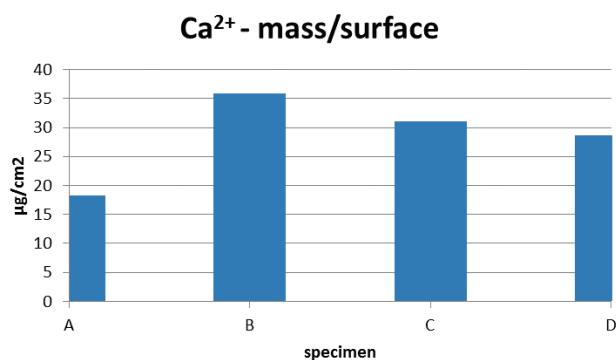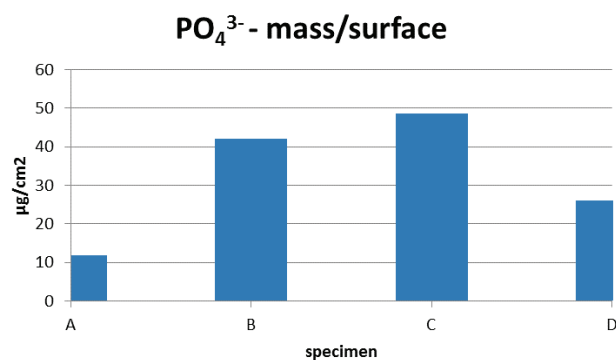

Fig. 8. Calcium mass/surface ratio
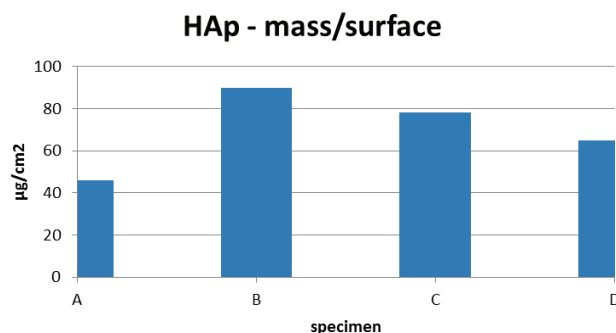on sensors inside porous structure

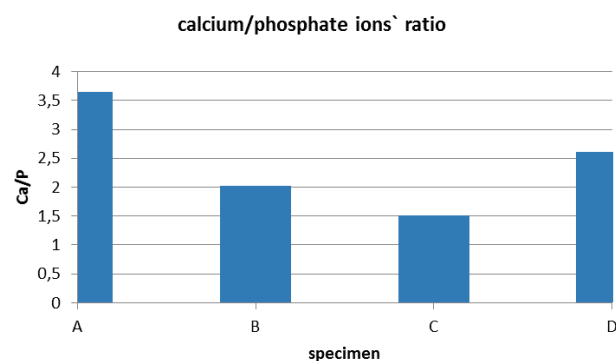Fig. 9. Hydroxyapatite mass/surface ratio
on sensors inside porous structure

Fig. 10. Ca^{2+}/PO_4^{3} mass/surface ratio
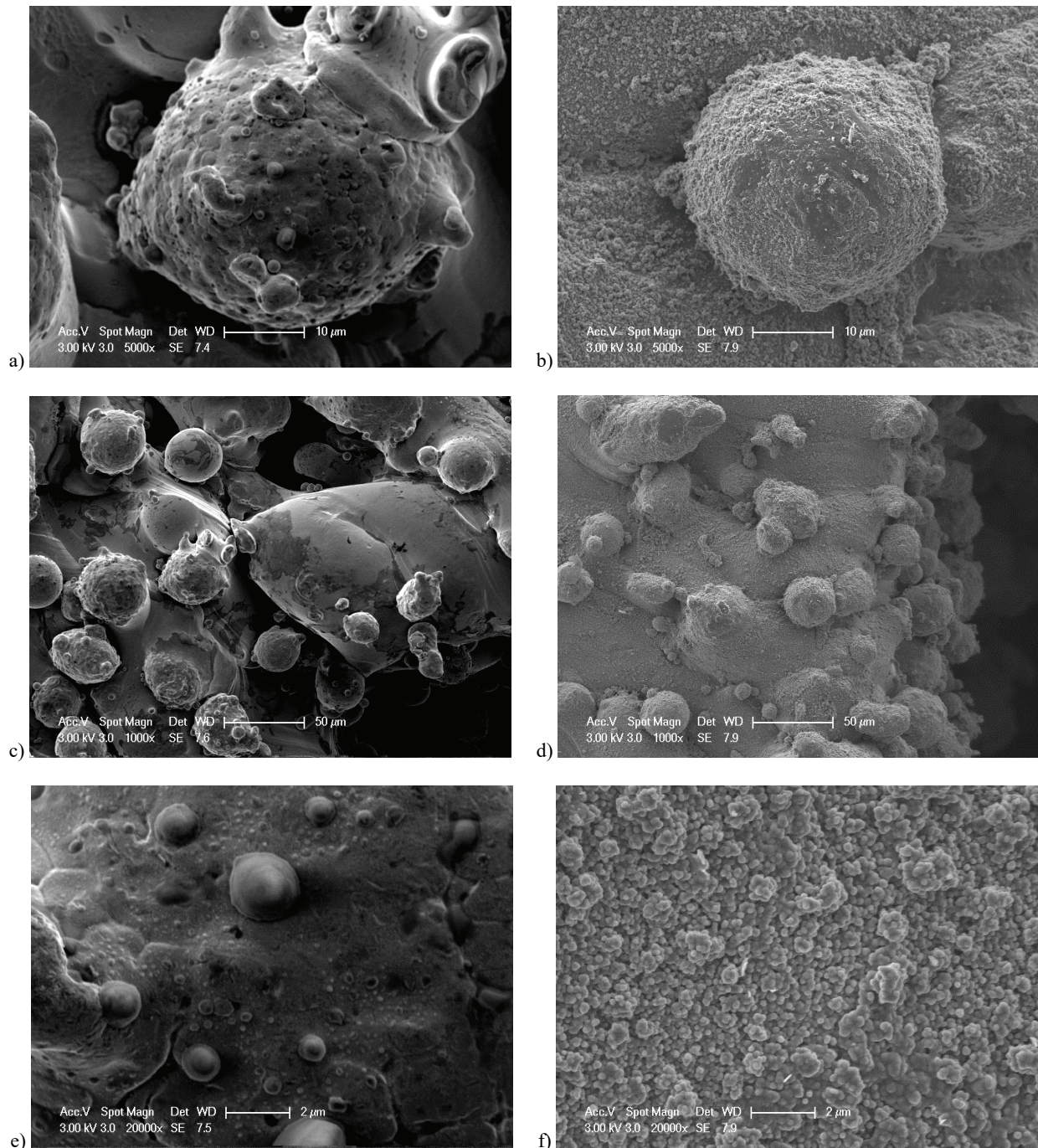on sensors inside porous structure

Fig. 11. Magnified views of the surfaces covered with calcium phosphate coating
after ECAD at –5 mA/cm^2 (a, c, e) and –8 mA/cm^2 (b, d, f) charging

4. Discussion

The deposition of phosphate and, particularly, hydroxyapatite coatings on the flat surfaces of Ti alloys, stainless steel, or Ti-Ni alloys has been clearly described. However, to date, for porous metals, the presence, thickness and properties of phosphate coatings obtained by electrochemical deposition inside the pores have rarely been investigated. In [26], for titanium beads with small diameters of 600–800 μm, porosity approaching 40%, and pore size ranging between 100 and 300 μm, deposits of 10–25 μm thickness were observed following biomimetic deposition and ECAD on the whole surface. For porous Co-Cr alloys produced by the additive technique with struts 330 μm and 640 μm, and with the biomimetic method used to deposit the phosphates over three days, thin

300–500-nm coatings were observed within a porous block 15 × 9 × 2.7 mm in size [14]. Our results are thus among the first to demonstrate that phosphate coatings can be obtained by the ECAD technique on a titanium surface deep inside porous structures.

The main obstacle to the formation of phosphate coatings inside porous structures is the difficulty of migration of substrates and products inside the pores. Another obstacle may include capillary effects resulting in a possible decrease in current value inside the holes. In our research as well as in previous studies [14], [26], these factors could not prevent the formation of phosphate coatings on Ti deep under the outer surface. The current value and distance from the surface may have had a certain effect, but this was slight or even insignificant within the limits of experimental error.

The resultant coatings in this research are characterised by a calcium/phosphate ratio which is higher than 1.67 and may approach as high as 2 to 2.5, suggesting that this coating is not a stoichiometric hydroxyapatite. The coating mass ranged from 33 to 62 $\mu g/cm^2$ (130 to 200 nm for stoichiometric HAp) for coatings deposited on isolated sensors and from 45 to 90 $\mu g/cm^2$ (170 to 300 nm for HAp) for sensors in porous structures. These results differ from those reported by Zhang et al. [26]. In their research, octacalcium phosphate (OCP) with a $Ca/PO4$ ratio of 1.33 was obtained inside the pores. The present results may be explained in terms of the migration of ions under ECAD conditions: migration into the scaffold pores of positively-charged Ca ions is enhanced by the applied cathodic current, but for negatively charged phosphate ions this phenomenon is impossible. As a consequence, the Ca^{2+}/PO_4^{3-} ratio in phosphate deposits is expected to increase in deep pores.

5. Conclusions

Calcium phosphate coatings can be deposited on a Ti surface even 50–140 mm inside the pores of a model scaffold made of 316L stainless steel. The thickness of these coatings, assessed by means of the coating mass measurements, ranges from 170 to 300 nm. The increase in cathodic current results in an increase in coating thickness.

The difference between the thickness of coatings on isolated Ti wires and Ti sensors placed inside the pores of the scaffold is relatively small. This observation demonstrates that the current values on the outer and inner surfaces are close so that any decrease in the cathodic current (screening effect) inside the porous structure is relatively low.

The calcium phosphate inside the pores has a much higher Ca/P ratio than that of stoichiometric HAp. This result may be explained by the differing effects of cathodic current on positively-charged calcium ions and negatively charged phosphate ions. This effect is presumed to result in a gradual increase in the Ca fraction with distance from the surface.

Acknowledgements

References

[1] ALBAYRAK O., EL-ATWANI O., ALTINTAS S., *Hydroxyapatite coating on titanium substrate by electrophoretic deposition method: effects of a titanium dioxide inner layer on adhesion strength and hydroxyapatite decomposition*, Surf. Coat. Technol., 2008, 202(11), 2482–2487, DOI: 10.1016/j.surfcoat.2007.09.031.

[2] BASALAH A., SHANJANI Y., ESMAEILI S., TOYSERKANI E., *Characterizations of additive manufactured porous titanium implants*, J. Biomed. Mater Res. B Appl. Biomater., 2012, 100(7), 1970–1979, DOI: 10.1002/jbm.b.32764.

[3] BRACCI B., PANZAVOLTA S., BIGI A., *A new simplified calcifying solution to synthesize calcium phosphate coatings*, Surf. Coat. Techn., 2013, 232, 13–21. DOI: 10.1016/j.surfcoat.2013.04.046.

[4] CHEN X.-B., LI Y.-C., DU PLESSIS J., HODGSON P. D., WEN C., *Influence of calcium ion deposition on apatite-inducing ability of porous titanium for biomedical applications*, Acta Biomater., 2009, 5(5), 1808–1820, DOI: 10.1016/j.actbio.2009.01.015.

[5] DEWIDAR M.M., KHALIL K.A., LIM J.K., *Processing and mechanical properties of porous 316L stainless steel for biomedical applications*, Trans. Nonferrous Met. So. China, 2007, 17, 468–473.

[6] GŁOGOCKA D., NOCULAK A., PUCIŃSKA J., JOPEK W., PODBIELSKA H., LANGNER M., PRZYBYŁO M., *Analysis of metal surfaces coated with europium-doped titanium dioxide by laser induced breakdown spectroscopy*, Acta Bioeng. Biomech., 2015, 17(3), 33–40, DOI: 10.5277/ABB-00138-2014-03.

[7] GU D., SHEN Y., *Processing conditions and microstructural features of porous 316L stainless steel components by DMLS*, Appl. Surf. Sci., 2008, 255(5), 1880–1887, DOI: 10.1016/j.apsusc.2008.06.118.

[8] JANSEN J.A., WOLKE J.G.C., SWANN S., VAN DER WAERDEN J.P.C.M., DE GROOF K., *Application of magnetron sputtering for producing ceramic coatings on implant material*, Clin. Oral. Impl. Res., 1993, 4(1), 28–34. DOI: 10.1034/j.1600-0501.1993.040104.x.

[9] KIM M.-S., JUNG U.-W., KIM S., LEE J.-S., LEE I.-S., CHOI S.-H., *Bone apposition on implants coated with calcium phosphate by ion beam assisted deposition in oversized drilled sockets: a histologic and histometric analysis in dogs*, J. Periodontal Implant Sci., 2013, 43(1), 18–23. DOI: 10.5051/jpis.2013.43.1.18.

[10] Koch C.F., Johnson S., Kumar D., Jelinek M., Chrisey D.B., Doraiswamy A., Jin C., Narayan R.J., Mihailescu I.N., *Pulsed laser deposition of hydroxyapatite thin films*, Mater. Sci. Eng. C, 2007, 27(3), 484–494, DOI: 10.1016/j.msec.2006.05.025.

[11] Kodama A., Bauer S., Komatsu A., Asoh H., Ono S., Schmuki P., *Bioactivation of titanium surfaces using coatings of TiO_2 nanotubes rapidly pre-loaded with synthetic hydroxyapatite*, Acta Biomater., 2009, 5(6), 2322–2330, DOI: 10.1016/j.actbio.2009.02.032.

[12] Li J.P., Habibovic P., van den Doel M., Wilson C.E., de Wijn J.R., van Blitterswijk C.A., de Groot K., *Bone in growth in porous titanium implants produced by 3D fiber deposition*, Biomaterials, 2007, 28, 2810–2820, DOI: 10.1016/j.biomaterials.2007.02.020.

[13] Lin W.S., Starr T.L., Harris B.T., Zandinejad A., Morton D., *Additive manufacturing technology (direct metal laser sintering) as a novel approach to fabricate functionally graded titanium implants: preliminary investigation of fabrication parameters*, Int. J. Oral. Maxillofac. Implants, 2013, 28(6), 1490–1495, DOI: 10.11607/jomi.3164.

[14] Lindahl C., Xia W., Engqvist H., Snis A., Lausmaa J., Palmquist A., *Biomimetic calcium phosphate coating of additively manufactured porous CoCr implants*, Appl. Surf. Sci., 2015, 353, 40–47. DOI: 10.1016/j.apsusc.2015.06.056.

[15] Mansur M.R., Wang J., Berndt C.C., *Microstructure, composition and hardness of laser-assisted hydroxyapatite and Ti-6Al-4V composite coatings*, Surf. Coat. Techn., 2013, 232, 482–488. DOI: 10.1016/j.surfcoat.2013.06.006.

[16] Mona Goudarzi M., Batmanghelich F., Afshar A., Dolati A., Mortazavi G., *Development of electrophoretically deposited hydroxyapatite coatings on anodized nanotubular TiO_2 structures: corrosion and sintering temperature*, Appl. Surf. Sci., 2014, 301, 250–257, DOI: 10.1016/j.apsusc.2014.02.055.

[17] Nelea V., Morosanu C., Iliescu M., Mihailescu I.N., *Microstructure and mechanical properties of hydroxyapatite thin films grown by RF magnetron sputtering*, Surf. Coat. Techn., 2003, 173(2–3), 315–322, DOI: 10.1016/S0257-8972(03)00729-1.

[18] Rainer A., Giannitelli S.M., Accoto D., De Porcellinis S., Guglielmelli E., Trombetta M., *Load-adaptive scaffold architecture: a bioinspired approach to the design of porous additively manufactured scaffolds with optimized mechanical properties*, Ann. Biomed. Eng., 2012, 40(4), 966–975, DOI: 10.1007/s10439-011-0465-4.

[19] Ribeiro A.A., Balestra R.M., Rocha M.N., Peripolli S.B., Andrade M.C., Pereira L.C., Oliveira M.V., *Dense and porous titanium substrates with a biomimetic calcium phosphate coating*, Appl. Surf. Sci., 2013, 265, 250–256, DOI: 10.1016/j.apsusc.2012.10.189.

[20] Roguska A., Pisarek M., Andrzejczuk M., Dolata M., Lewandowska M., Janik-Czachor M., *Characterization of a calcium phosphate–TiO_2 nanotube composite layer for biomedical applications*, Mater Sci. Eng. C, 2011, 39(5), 906–914, DOI: 10.1016/j.msec.2011.02.009.

[21] Rößler S., Sewing A., Stolzel M., Born R., Scharnweber D., Dard M., Worch H., *Electrochemically assisted deposition of thin calcium phosphate coatings at near-physiological pH and temperature*, J. Biomed. Mater Res. A, 2003, 64(4), 655–636, DOI: 10.1002/jbm.a.10330.

[22] Rumian Ł., Reczyńska K., Wrona M., Tiainen H., Haugen H. J., Pamuła E., *The influence of sintering conditions on microstructure and mechanical properties of titanium dioxide scaffolds for the treatment of bone tissue defects*, Acta Bioeng. Biomech., 2015, 17(1), 3–9, DOI: 10.5277/ABB-00129-2014-02.

[23] Ryan G., Pandit A., Apatsidis D.P., *Fabrication methods of porous metals for use in orthopedic applications*, Biomaterials, 2006, 27(13), 2651–2670, DOI: 10.1016/j.biomaterials.2005.12.002.

[24] Wang L.-N., Luo J.-L., *Fabrication and formation of bioactive anodic zirconium oxide nanotubes containing presynthesized hydroxyapatite via alternative immersion method*, Mater Sci. Eng. C, 2011, 31(4), 748–754, DOI: 10.1016/j.msec.2010.10.008.

[25] Xie F., He X., Cao S., Qu X., *Structural and mechanical characteristics of porous 316L stainless steel fabricated by indirect selective laser sintering*, J. Mater Proc. Techn., 2013, 213(6), 838–843, DOI: 10.1016/j.jmatprotec.2012.12.014.

[26] Zhang Q., Leng Y., Xin R., *A comparative study of electrochemical deposition and biomimetic deposition of calcium phosphate on porous titanium*, Biomaterials, 2005, 26(16), 2857–2865, DOI: 10.1016/j.biomaterials.2004.08.016.

[27] Zieliński A., Antoniuk P., Krzysztofowicz K., *Nanotubular oxide layers and hydroxyapatite coatings on "Ti–13Zr–13Nb" alloy*, Surf. Eng., 2014, 30(9), 643–649, DOI: 10.1179/1743294414Y.0000000302.